SIAM J. APPL. MATH.
Vol. 64, No. 3, pp. 977–1001
© 2004 Society for Industrial and Applied Mathematics

DISPERSIVE WAVE ATTENUATION DUE TO OROGRAPHIC FORCING*

JUAN CARLOS MUÑOZ GRAJALES† AND ANDRÉ NACHBIN‡

Abstract. The O'Doherty–Anstey (ODA) approximation was originally formulated in the seismological literature for acoustic pulse propagation through a disordered stratified medium [*Geophys. Prospecting*, 19 (1971), pp. 430–458]. It explains the mechanism for amplitude attenuation (and pulse shaping) promoted by the variable coefficient, conservative hyperbolic model. This work generalizes the one-dimensional ODA theory for linear weakly dispersive water waves forced by a disordered orography. The analysis is performed through the recently formulated terrain-following Boussinesq system. This is achieved by applying the invariant imbedding method. As a result, dispersion alters the medium's correlation function which controls the apparent attenuation mechanism. On the other hand, orography affects the dispersive mechanism for the Airy function–like formation. A nonlinear Boussinesq solver was implemented, and theoretical results were validated for different values of the parameters of interest. The theoretical results are in very good agreement with the small amplitude simulations. In particular, the approximate theory was able to capture a good part of the forward scattering radiation. Moreover, through numerical experiments the theory is pushed beyond its expected regime and captures the attenuation of small amplitude solitons due to orographic forcing.

Key words. dispersive waves, inhomogeneous media, asymptotic theory

AMS subject classifications. 76B07, 76B15, 35Q

DOI. 10.1137/S0036139902412769

1. Introduction.

Wave-topography interaction has been the subject of considerable mathematical research. The physical applications range from coastal surface waves [18] to atmospheric flows over mountain ranges [2, 7]. In particular, the interaction of waves with fine features of the topography is of great interest. As pointed out in the introduction to [7], the "representation ... of subgrid-scale orographic processes is recognized as crucial to numerical weather prediction at all time ranges." In the atmospheric literature *orography* implies mountain ranges [2]. Our study is therefore focused on the effect of small-scale orographic features, which we call the *microstructure*. A mathematical theory is described and its robustness validated numerically. As surface gravity waves propagate from deep to shallow waters, they are transformed due to shoaling, refraction, diffraction, and reflection. In order to concentrate on the main scattering mechanism connected with the pulse shaping phenomenon to be described, we consider the normal incidence of surface pulse shaped waves. These waves propagate over topographies containing a smooth slowly varying profile together with disordered small-scale features. Our goal is to capture the wave-microstructure interaction.

The main result is that the disordered medium fluctuations cause the propagating pulse to broaden as it travels. Due to multiple scattered energy, the pulse appears to

*Received by the editors August 6, 2002; accepted for publication (in revised form) September 25, 2003; published electronically March 30, 2004. This work was supported by CNPq/Brazil under grant 300368/96-8. Part of this work was supported by NSF grant DMS97-09320 through the Mathematical Geophysics Summer Schools (1998–2002) at Stanford University.

http://www.siam.org/journals/siap/64-3/41276.html

†Instituto de Matemática Pura e Aplicada, Est. D. Castorina 110, Jardim Botânico, Rio de Janeiro, RJ 22460-320, Brazil (juanc@impa.br). Current address: Department of Mathematics, Universidad del Valle, A. A. 25360, Cali, Colombia.

‡Instituto de Matemática Pura e Aplicada, Est. D. Castorina 110, Jardim Botânico, Rio de Janeiro, RJ 22460-320, Brazil (nachbin@impa.br).

diffuse about a moving center. The amount of broadening and attenuation is proportional to the traveling distance and depends on the disorder's correlation function. In what follows we refer to the transformation of the pulse due to the medium's microscale fluctuations as *pulse shaping*.

The theory for pulse shaping was originally derived in the context of acoustic wave propagation in the earth's crust [25]. It is known as the O'Doherty–Anstey (ODA) approximation. In the acoustic wave applications several authors have analyzed the spreading of a pulse due to microscale variations in the medium parameters (cf., for example, the work by Clouet and Fouque [9], Papanicolaou and Sølna [27], and Lewicki, Burridge, and de Hoop [15]). The motivation for modeling in terms of a random medium is that a detailed description of microscale medium fluctuations is often not known. Using a stochastic model, uncertainties about a specific medium are translated into uncertainties about a transmitted pulse shape in a systematic way [1]. Stochastic modeling has been used by Nachbin for long weakly dispersive surface wave problems [22, 24].

This work generalizes the one-dimensional ODA theory for linear weakly dispersive water waves when forced by a disordered orography. The analysis is performed through the recently formulated terrain-following Boussinesq system [23]. This is achieved by applying the invariant imbedding method. As a result, dispersion alters the medium's correlation function, which controls the apparent attenuation mechanism. On the other hand, orography affects the dispersive mechanism for the Airy function–like formation. A nonlinear Boussinesq solver was implemented, and theoretical results were validated for different values of the parameters of interest. Details of the numerical method and a larger range of experiments will be presented elsewhere [20]. The theoretical results presented here are in very good agreement with the small amplitude simulations. This amounts to solving the nonlinear Boussinesq system with data on a small amplitude-to-depth ratio. In particular, the approximate theory was able to capture a good part of the forward scattering radiation.

This paper is organized as follows. In section 2 we present the terrain-following Boussinesq system. In section 3 the pulse shaping ODA theory is formulated in detail. Section 4 contains five sets of numerical experiments validating the theory and generating further insight into it. The conclusions are given in section 5. A three-part appendix is intended to provide further detail for the reader.

2. The linearized terrain-following Boussinesq model. We start by presenting the potential theory formulation for Euler's equations with a free surface and an impermeable bottom topography. In the potential theory model the fluid is assumed to be inviscid, incompressible, and irrotational. Let variables with physical dimensions be denoted with a tilde. We introduce the length scales σ (a typical pulse width or wavelength), h_0 (a typical depth), a (a typical wave amplitude), ℓ (the horizontal length scale for bottom irregularities), and L (the total length of the rough region or the total propagation distance). The acceleration due to gravity is denoted by g, and the reference shallow water speed is $c_0 = \sqrt{gh_0}$. Dimensionless variables are then defined in a standard fashion [23, 29]:

$$\tilde{x} = \sigma x, \quad \tilde{y} = h_0\, y, \quad \tilde{t} = \left(\frac{\sigma}{c_0}\right) t, \quad \tilde{\eta} = a\, \eta, \quad \tilde{\phi} = \left(\frac{g\sigma a}{c_0}\right) \phi, \quad \tilde{h} = h_0\, H\left(\frac{\tilde{x}}{\ell}\right).$$

The velocity potential $\phi(x, y, t)$ and wave elevation $\eta(x, t)$ satisfy the dimensionless equations (see [29])

$$\beta\, \phi_{xx} + \phi_{yy} = 0 \quad \text{for} \quad -H(x/\gamma) < y < \alpha\eta(x, t),$$

with the nonlinear free surface conditions

$$\eta_t + \alpha\phi_x\eta_x - \frac{1}{\beta}\phi_y = 0,$$

$$\eta + \phi_t + \frac{\alpha}{2}\left(\phi_x^2 + \frac{1}{\beta}\phi_y^2\right) = 0$$

at $y = \alpha\eta(x,t)$. The parameter $\alpha = a/h_0$ controls the strength of nonlinear effects, and $\beta = h_0^2/\sigma^2$ the level of dispersion. The length scale for the bottom inhomogeneities ℓ leads to the dimensionless parameter $\gamma = \ell/\sigma$. The Neumann condition at the impermeable bottom is

$$\phi_y + \frac{\beta}{\gamma}\, H'(x/\gamma)\phi_x = 0.$$

The bottom topography is described by $y = -H(x/\gamma)$, where

$$H(x/\gamma) \;=\; \begin{cases} 1 + n(x/\gamma) & \text{when } \; 0 < x < L, \\ 1 & \text{when } \; x \le 0 \;\text{ or }\; x \ge L. \end{cases}$$

The bottom profile is described by the function $-n(x/\gamma)$. The topography is rapidly varying when $\gamma \ll 1$. The undisturbed depth is given by $y = -1$, and the topography can be of large amplitude, provided that $|n| < 1$. We do not need to assume that the fluctuations n are small, nor continuous, nor slowly varying.

In past years Boussinesq-type equations have been employed to model surface wave propagation in shallow channels. Such models are weakly nonlinear, weakly dispersive approximations to the full potential theory equations. Peregrine [26] in 1967 deduced a model valid for channels of slowly varying depth, whereas Hamilton [14] in 1977 derived a set of equations valid for arbitrary orographies. The latter used an appropriate curvilinear coordinate system and applied a perturbation approach to the linear potential theory equations retaining the lowest-order effects of dispersion. The change of variables uses a conformal mapping from a strip in the complex $(\xi, \tilde{\zeta})$-plane to the complex z-plane ($z = x + i\tilde{y}$; $\tilde{y} \equiv \beta^{1/2} y$) (see [23]). Hamilton also outlines the formulation of a weakly nonlinear model by considering a Lagragian functional. In this direction, using dimensionless variables and Hamilton's conformal mapping strategy, the potential theory equations are first cast in a fixed orthogonal curvilinear coordinates $(\xi, \tilde{\zeta})$ as (see [23])

$$\phi_{\xi\xi} \;+\; \phi_{\tilde{\zeta}\tilde{\zeta}} \;=\; 0, \qquad\qquad -\sqrt{\beta} < \tilde{\zeta} < \alpha\sqrt{\beta}N(\xi,t), \tag{2.1}$$

with free surface conditions

$$|J|N_t + \alpha\phi_\xi N_\xi - \frac{1}{\sqrt{\beta}}\phi_{\tilde{\zeta}} = 0 \tag{2.2}$$

and

$$\phi_t + \eta + \frac{\alpha}{2|J|}\left(\phi_\xi^2 + \phi_{\tilde{\zeta}}^2\right) = 0 \tag{2.3}$$

at $\tilde{\zeta} = \alpha\sqrt{\beta}N(\xi,t)$. The bottom condition is

$$\phi_{\tilde{\zeta}} = 0 \qquad \text{at } \; \tilde{\zeta} = -\sqrt{\beta}. \tag{2.4}$$

The Jacobian for the $(\xi, \tilde{\zeta}) \to (x, \tilde{y})$ coordinate transformation is represented by $|J|$. Details can be found in Nachbin [23], where the potential theory equations given above are approximated as the ($O(\alpha)$, $O(\beta)$: respectively, weakly nonlinear, weakly dispersive) terrain-following Boussinesq system

$$M(\xi)\eta_t + \left(\left(1 + \frac{\alpha\eta}{M(\xi)}\right)u\right)_\xi = 0,$$
$$u_t + \eta_\xi + \frac{\alpha}{2}\left(\frac{u^2}{M(\xi)^2}\right)_\xi - \frac{\beta}{3}u_{\xi\xi t} = 0.$$

The metric term $M(\xi)$ is defined by

$$M(\xi) \equiv \tilde{y}_{\tilde{\zeta}}(\xi, 0).$$

When $\alpha = 0$ the system above reduces to

$$M(\xi)\eta_t + u_\xi = 0, \tag{2.5}$$
$$u_t + \eta_\xi - \frac{\beta}{3}u_{\xi\xi t} = 0.$$

Here ξ and t are the space and time coordinates, respectively; $\eta = \eta(\xi, t)$ is the wave elevation; and $u = u(\xi, t)$ is the weighted depth-averaged terrain-following velocity [23]. The variable coefficient $M(\xi)$ is a smooth orography-dependent function which appears as a consequence of the changes of variables [23]. When the parameter β is small, we are in the shallow channel/long wave regime. Equivalently, this is called the weakly dispersive regime.

In the next section we will analyze the linear ($\alpha = 0$) Boussinesq system for a large range of dispersive effects, expressed through the parameter β. It is very important to note that for $\beta > 0.25$ we are in the *deep water* regime. The particle-orbits decay exponentially with depth as shown in Dean and Dalrymple [5, Chapter 4, on linear potential theory]. Hence in this regime there is no wave-topography interaction. Thus the fact that the Boussinesq system is an $O(\beta)$ approximation to the potential theory is not much of a limitation for dispersive wave-topography interaction. Moreover, for large time intervals dispersive effects will be strongly displayed in the solutions even for small values of β (cf. Appendix A). Even though the theory we have developed is linear, in our numerical experiments we will consider nontrivial values of α, as will be discussed in the corresponding subsections.

3. The linear pulse shaping theory. In this section we generalize the ODA approximation from linear acoustic waves to the linear weakly dispersive system (2.5). The weakly dispersive Boussinesq system is forced by a rapidly varying orography expressed through the variable coefficient $M(\xi)$. We consider a technique analogous to Berlyand and Burridge's acoustic work [3], which we apply successfully to dispersive waves for two reasons. First, system (2.5) can be written equivalently as two coupled KdV-type equations for the transmitted and reflected fields. These linearized KdV-type equations can be viewed as a dispersive perturbation to those obtained by Berlyand and Burridge; namely, a propagating pulse will slowly disperse with a given (known) rate (cf. Appendix A, (A.4)). Second, the pulse's effective propagation velocity is bounded, and all Fourier modes have positive phase speeds bounded by 1. These two properties described allow us to apply the *invariant imbedding approach* [19], taking the propagation distance as the *imbedding parameter*.

In what follows, solutions u, η to (2.5) will be assumed to be smooth enough and absolutely integrable. This requirement is necessary to justify the use of the Fourier transform and the Fourier inversion formula.

We start by performing the change of variables

$$x = \int_0^{\xi} \frac{1}{C_o(s)} ds, \quad t' = t$$

in system (2.5). Here $C_o(s) = \sqrt{1/M(s)}$ is the *local wave speed* and x is the *travel time*. Dropping the primes, system (2.5) becomes

$$\begin{aligned} & C_o^{-1/2}\, \eta_t + C_o^{1/2}\, u_x = 0, \\ & C_o^{1/2}\, u_t + C_o^{-1/2}\, \eta_x - \frac{\beta}{3C_o^{1/2}} \left(u_{xxt}\, \frac{1}{C_o} + \left(\frac{1}{C_o} \right)_x u_{xt} \right) = 0. \end{aligned} \tag{3.1}$$

We adopt the *wave mode splitting*

$$R = C_o^{1/2} u + C_o^{-1/2} \eta, \tag{3.2}$$

$$L = -C_o^{1/2} u + C_o^{-1/2} \eta. \tag{3.3}$$

Differentiating (3.2) and (3.3) with respect to x and t and using (3.1) and the fact that $u = (R - L)/(2C_o^{1/2})$ leads to the coupled wave mode system

$$\begin{aligned} R_t + R_x &= p(x) \left(\frac{R - L}{2C_o^{1/2}} \right)_{xxt} + q(x) \left(\frac{R - L}{2C_o^{1/2}} \right)_{xt} - r(x) L, \\ L_x - L_t &= p(x) \left(\frac{R - L}{2C_o^{1/2}} \right)_{xxt} + q(x) \left(\frac{R - L}{2C_o^{1/2}} \right)_{xt} - r(x) R, \end{aligned} \tag{3.4}$$

where the variable coefficients are

$$p(x) = \frac{\beta}{3C_o^{3/2}(x)}, \quad q(x) = -\frac{\beta C_{o,x}(x)}{3C_o^{5/2}(x)}, \quad \text{and} \quad r(x) = \frac{C_{o,x}(x)}{2C_o(x)}.$$

The initial conditions for system (3.4) are

$$R(x, 0) = R_o(x), \quad L(x, 0) = 0.$$

Note that when the bottom is flat ($r \equiv 0$) and $\beta = 0$ (no dispersion), equations (3.4) identify R with a wave propagating to the right (transmitted wave) and L with a wave propagating to the left (reflected wave). For variable depths we adopt the same terminology. Moreover, this terminology is also consistent for system (3.4), in the weakly dispersive regime ($0 < \beta \ll 1$) and $r \equiv 0$, since the left-propagating signal L is negligible if the initial data corresponds to a right-going wave (see Appendix A).

Several decompositions of the Boussinesq equations into a pair of KdV equations were introduced by Mattioli in [16] and [17]. We point out that system (3.4) has some advantages with respect to those decompositions. First, unlike system (3.4), the Boussinesq equations used by Mattioli are not valid as an asymptotic approximation of the potential theory equations for arbitrary rapidly varying or nondifferentiable orographies. Second, in contrast to system (3.4), the linear dispersion relation for Mattioli's model results in unstable short waves with amplitude tending to infinity.

In order to set our forthcoming results in a wave propagating frame let us introduce the change of variables

$$\tau = t - x, \quad x' = x,$$

where τ is the time-delay variable. Again abandoning the primes, equations (3.4) become

$$\begin{aligned} R_x = {} & p\left(\frac{R-L}{2C_o^{1/2}}\right)_{\tau\tau\tau} - 2p\left(\frac{R-L}{2C_o^{1/2}}\right)_{x\tau\tau} + p\left(\frac{R-L}{2C_o^{1/2}}\right)_{xx\tau} \\ & - q\left(\frac{R-L}{2C_o^{1/2}}\right)_{\tau\tau} + q\left(\frac{R-L}{2C_o^{1/2}}\right)_{x\tau} - rL, \\ L_x - 2L_\tau = {} & p\left(\frac{R-L}{2C_o^{1/2}}\right)_{\tau\tau\tau} - 2p\left(\frac{R-L}{2C_o^{1/2}}\right)_{x\tau\tau} + p\left(\frac{R-L}{2C_o^{1/2}}\right)_{xx\tau} \\ & - q\left(\frac{R-L}{2C_o^{1/2}}\right)_{\tau\tau} + q\left(\frac{R-L}{2C_o^{1/2}}\right)_{x\tau} - rR. \end{aligned} \tag{3.5}$$

Let $\widehat{f}(\omega)$ denote the Fourier transform of $f(\tau)$ in the time-delay variable τ:

$$\widehat{f}(\omega) = \int_{-\infty}^{\infty} e^{-i\omega\tau} f(\tau)\, d\tau.$$

Take the Fourier transform in τ of (3.5). Manipulate the resulting system in order to obtain first-order equations for the travel time-evolution of the Fourier modes. This goal is achieved by first subtracting the two equations giving

$$\widehat{R}_x - \widehat{L}_x = r\widehat{R} - 2i\omega\widehat{L} - r\widehat{L}. \tag{3.6}$$

Moreover, by differentiating this equation with respect to x, we find

$$\begin{aligned} \widehat{R}_{xx} - \widehat{L}_{xx} = {} & r'(x)\widehat{R} - r'(x)\widehat{L} - 2iw\widehat{R}_x + 2iwr(x)\widehat{R} \\ & + 4w^2\widehat{L} - 4iwr(x)\widehat{L} + r^2(x)\widehat{R} - r^2(x)\widehat{L}. \end{aligned} \tag{3.7}$$

This expression can be used to eliminate the second order x-derivatives in the first Fourier transformed equation arising from (3.5). This is a crucial step in order to apply the invariant imbedding approach, which requires a first-order system of ordinary differential equations (ODE). Using the fact that the time frequency range $|\omega| < C_o(x)\sqrt{3/\beta}$ (see Appendix A), we solve for $\widehat{R}_x$ to obtain

$$\widehat{R}_x = \zeta(x,\omega)\widehat{L} + \gamma(x,\omega)\widehat{R}, \tag{3.8}$$

where

$$\zeta(x,\omega) = \frac{id(x)\omega^3 + e(x)\omega^2 - 2r(x)}{2(1 - d(x)\ \omega^2)}, \quad \gamma(x,\omega) = \frac{\frac{-i\beta\omega^2}{3C_o^2(x)}(\omega - 4ir(x))}{2\left(1 - \frac{\beta\omega^2}{3C_o^2(x)}\right)},$$

$$d(x) = \frac{\beta}{3C_o^2(x)} \quad \text{and} \quad e(x) = -\frac{\beta}{3C_o^3(x)}C_{o,x}(x).$$

Putting (3.8) into (3.6) and solving for $\widehat{L}_x$ results in

$$\widehat{L}_x = (2i\omega + \bar{\gamma}(x,\omega))\widehat{L} + \bar{\zeta}(x,\omega)\widehat{R}, \tag{3.9}$$

where $\bar{\zeta}(x,w)$ and $\bar{\gamma}(x,w)$ denote the complex conjugates of $\zeta(x,w)$ and $\gamma(x,w)$, respectively. As claimed above, (3.8) and (3.9) give the evolution in x (travel time) of each Fourier mode, corresponding to the transmitted and reflected fields.

Next, suppose that we want to calculate $L(x_o,\tau) = L(x_o,\tau;T)$ for $0 \le \tau \le T$. At this step we apply the *invariant imbedding approach* [19] to system (3.8) and (3.9). To do so we imbed the relevant inhomogeneous region inside a homogeneous medium so that we can give appropriate boundary conditions at the border of the medium's slab $[x_o, x_o + X]$, say

$$\widehat{R}(x_o,\omega;T) = \widehat{h}(\omega), \tag{3.10}$$

$$\widehat{L}(x_o + X,\omega;T) = 0. \tag{3.11}$$

Boundary condition (3.11) means that no reflection is expected at the downstream travel time location x_o+X when $0 < \tau = t - x_o < T$. In other words, the signal did not have enough time to arrive at this point and to produce a medium's response. This is true at least for some $X > 0$ large enough (depending on T) due to the pulse's finite (effective) velocity mentioned earlier. Linearity of ODE system (3.8)–(3.9) and the invariant imbedding technique [19] guarantees the existence of a function $K(x,\omega;T)$ (called the *reflection kernel*) such that

$$\widehat{L}(x,\omega;T) = \widehat{K}(x,\omega;T)\ \widehat{R}(x,\omega;T) \tag{3.12}$$

and satisfying the Riccati-type equation

$$\widehat{K}_x = \bar{\zeta}(x,\omega) + 2i\omega\Gamma(x,\omega)\widehat{K} - \zeta(x,\omega)\widehat{K}^2, \tag{3.13}$$

with

$$\Gamma(x,\omega) = \frac{2 - d(x)\omega^2}{2(1 - d(x)\omega^2)}.$$

From (3.11) we obtain an appropriate initial condition for (3.13):

$$\widehat{K}(x_o + X,\omega;T) = 0. \tag{3.14}$$

Notice that (3.12) allows us to solve for the reflected signal $L(x_o,\tau;T)$ in terms of the reflection kernel $K(x_o,\tau;T)$ and the transmitted pulse $R(x_o,\tau;T)$ for $0 \le \tau \le T$. This function K contains all the information about medium's reflection properties. We also remark that the boundary value problem (3.8), (3.9), (3.10), (3.11) has been reduced to solving the initial value problem (3.13)–(3.14) in reversed direction from the travel time location $x_o + X$ up to the time of interest x_o.

In general it is not possible to solve explicitly for $\widehat{K}$ from (3.13), so we adopt an approximation. To this end we present the following generalization to the lemma given by Berlyand and Burridge [3].

LEMMA 3.1. *Let y satisfy the Riccati equation*

$$y'(s) = -A(s) - 2i\omega B(s)y(s) + \bar{A}(s)y^2(s), \quad 0 \le s \le s_o, \tag{3.15}$$

subject to the initial condition $y(0) = 0$. *Here* $\bar{A}(s)$ *denotes the complex conjugate of* $A(s)$. *Hence the solution can be expressed as*

$$y(s_o) = -\int_0^{s_o} e^{-2i\omega \int_{s'}^{s_o} B(\xi)d\xi} A(s')ds' + E(s_o), \tag{3.16}$$

where the error term is

$$E(s_o) = \int_0^{s_o} \bar{A}(s') e^{-2i\omega \int_{s'}^{s_o} B(\xi)d\xi} y^2(s')ds'.$$

Set

$$v(s_o) = \sup_{0\le s\le s_o} \left| \int_0^s e^{2iw \int_0^{s'} B(\xi)d\xi} A(s')ds' \right| \quad \textit{and} \quad V(s) = \int_0^s |A(s')|\, ds'.$$

If $v(s_o)V(s) < 1$, *then*

$$|E(s)| \le \frac{v^2(s_o)V(s)}{1 - v(s_o)V(s)}, \quad 0 \le s \le s_o. \tag{3.17}$$

Proof. Multiplying (3.15) by its integrating factor and integrating both sides from 0 to s yields

$$\begin{aligned} &\int_0^s e^{2i\omega \int_0^{s'} B(\xi)d\xi} y'(s')ds' + 2iw \int_0^s B(s') e^{2i\omega \int_0^{s'} B(\xi)d\xi} y(s')ds' \\ &= -\int_0^s e^{2iw \int_0^{s'} B(\xi)d\xi} A(s')ds' + \int_0^s \bar{A}(s') e^{2i\omega \int_0^{s'} B(\xi)d\xi} y^2(s')ds'. \end{aligned}$$

Consequently,

$$\begin{aligned} &\int_0^s \frac{d}{ds'} \left(e^{2i\omega \int_0^{s'} B(\xi)d\xi} y(s') \right) ds' = e^{2i\omega \int_0^s B(\xi)d\xi} y(s) \\ &= -\int_0^s e^{2i\omega \int_0^{s'} B(\xi)d\xi} A(s')ds' + \int_0^s \bar{A}(s') e^{2i\omega \int_0^{s'} B(\xi)d\xi} y^2(s')ds'. \end{aligned} \tag{3.18}$$

Now solving for $y(s)$ and evaluating at $s = s_o$, in (3.18) we arrive at (3.16).

To achieve estimate (3.17) we start with

$$\begin{aligned} E(s) &= \int_0^s \bar{A}(s') e^{-2i\omega \int_{s'}^{s} B(\xi)d\xi} y^2(s')ds' \\ &= e^{-2i\omega \int_0^s B(\xi)d\xi} \int_0^s \bar{A}(s') e^{2i\omega \int_0^{s'} B(\xi)d\xi} y^2(s')ds'. \end{aligned}$$

Let

$$Y(s) = \int_0^s |A(s')|\, |y(s')|^2\, ds'. \tag{3.19}$$

Hence

$$|E(s)| = \left| \int_0^s \bar{A}(s') e^{2i\omega \int_0^{s'} B(\xi)d\xi} y^2(s')ds' \right| \le Y(s). \tag{3.20}$$

Differentiating (3.19) with respect to s,

$$Y'(s) = |A(s)|\,|y(s)|^2. \tag{3.21}$$

Note that from (3.16) and (3.20)

$$|y(s)| \le v(s_o) + Y(s), \quad 0 \le s \le s_o. \tag{3.22}$$

Thus substituting (3.22) into (3.21) leads to

$$Y'(s) \le |A(s)|\,(v(s_o) + Y(s))^2. \tag{3.23}$$

By integrating (3.23) from 0 to s, we obtain

$$\int_0^s \frac{Y'(s)}{(v(s_o) + Y(s'))^2} ds' \le \int_0^s |A(s')|\, ds' = V(s).$$

Therefore,

$$\frac{1}{v(s_o)} - \frac{1}{v(s_o) + Y(s)} \le V(s).$$

Thus if $v(s_o)V(s) < 1$, equation (3.20) gives

$$|E(s)| \le Y(s) \le \frac{v^2(s_o)V(s)}{1 - v(s_o)V(s)}, \quad 0 \le s \le s_o.$$

This concludes the lemma's proof. □

We now apply these results to our Riccati equation. For brevity the argument T will be omitted in what follows. We apply the lemma above to the reflection kernel's problem (3.13)–(3.14) by letting $y(s) = \widehat{K}(x(s), \omega)$, $A(s) = \bar{\zeta}(x(s), \omega)$, $B(s) = \Gamma(x(s), \omega)$, and $s = x_o + X - x$, $s_o = X$. We deduce that

$$\widehat{K}(x, \omega) = -\int_x^{x+X} e^{2i\omega \int_{x'}^{x} \Gamma(s,\omega)\, ds} \bar{\zeta}(x', \omega) dx' + E(x, \omega), \tag{3.24}$$

with an error term given by

$$E(x, \omega) = \int_x^{x+X} e^{2i\omega \int_{x'}^{x} \Gamma(s,\omega)\, ds} \zeta(x', \omega) \widehat{K}^2(x', \omega) dx'.$$

Also

$$v(x_o, \omega) = \sup_{x_o \le x \le x_o + X} \left| \int_x^{x_o+X} e^{2i\omega \int_{x'}^{x_o+X} \Gamma(s,\omega)\, ds} \bar{\zeta}(x', \omega) dx' \right|$$

and

$$V(x_o, \omega) = \int_{x_o}^{x_o+X} |\zeta(x', \omega)|\, dx'.$$

Then, in the cases where $v(x_o, \omega)V(x_o, \omega) < 1$, the error bound follows.

Now we solve for $\widehat{R}(x_o,\omega)$ at an arbitrary point x_o by using (3.24) and (3.12) in (3.8). It results that

$$\widehat{R}_x(x,\omega)=\left(\zeta(x,\omega)\left(-\int_x^{x+X} e^{2i\omega\int_{x'}^{x}\Gamma(s,\omega)\,ds}\bar{\zeta}(x',\omega)dx'+E(x,\omega)\right)+\gamma\right)\ \widehat{R}(x,\omega).$$

Solving this initial value problem with $\widehat{R}(0,\omega)=\widehat{f}(\omega)$, then

$$\widehat{R}(x_o,\omega)=\widehat{f}(\omega)\ \exp\left[-\int_0^{x_o}\int_x^{x+X}\zeta(x,\omega)e^{2i\omega\ \int_{x'}^{x}\Gamma(s,\omega)\,ds}\ \bar{\zeta}(x',\omega)dx'+\gamma(x,\omega)\ dx\right]$$

$$\cdot\exp\left[\int_0^{x_o}\zeta(x,\omega)\ E(x,\omega)\,dx\right]. \tag{3.25}$$

For general rapidly varying orographies and $\beta\ll 1$ the error function $E(x,\omega)$ is small (see Appendix C), even though the error estimate (3.17) is not useful in this case. Estimate (3.17) is sharp, for instance, when the function describing the medium properties (the metric coefficient $M(x)$ in system (2.5)) is taken to be piecewise constant on travel-time intervals with equal length (called a *Goupillaud medium*) [21].

Therefore, (3.25) leads to the *generalized ODA approximation*

$$\widehat{R}(x_o,\omega)\approx\widehat{f}(\omega)e^{-x_o(a_\beta(x_o,\omega)+b(x_o,\omega))}, \tag{3.26}$$

where

$$a_\beta(x_o,\omega)=\frac{1}{x_o}\int_0^{x_o}\int_x^{x+X}\zeta(x,\omega)e^{2i\omega\int_{x'}^{x}\Gamma(s,\omega)\,ds}\bar{\zeta}(x',\omega)dx'\,dx, \tag{3.27}$$

$$b(x_o,\omega)=-\frac{1}{x_o}\int_0^{x_o}\gamma(x,\omega)\,dx. \tag{3.28}$$

Using approximation (3.26), we can obtain an expression for $R(x_o,\tau)$ (the transmitted field in our applications) by using the Fourier inversion formula. Thus for $0\le\tau\le T$

$$R(x_o,\tau)\approx\frac{1}{2\pi}\int_{-\infty}^{\infty}\widehat{f}(\omega)e^{-x_o(a_\beta(x_o,\omega)+b(x_o,\omega))}e^{i\omega\tau}d\omega. \tag{3.29}$$

Note that the exponential factor in (3.29) accounts for the wave attenuation at travel time x_o. As mentioned above, the error estimate given above is not always sharp. For this reason the error term $E(x_o,\omega)$ is calculated numerically in Appendix C. Furthermore, for dispersion parameter β small enough and constant depth ($r(x)\equiv 0$) we have that $a_\beta=O(\beta^2)$ and $b=O(\beta)$. Hence for variable depths it is reasonable to approximate the medium's dispersive correlation function $a_\beta(x_o,\omega)$ by the medium's hyperbolic correlation function $a_0(x_o,\omega)$; that is,

$$a_\beta(x_o,\omega)\approx\frac{1}{x_o}\int_0^{x_o}\int_x^{x+X}r(x)e^{2i\omega(x-x')}r(x')dx'\ dx\equiv a_0(x_o,\omega). \tag{3.30}$$

This approximation, valid for small values of β, is not a limitation of the theory but enables numerical efficiency in the evaluation of the Fourier integrals. Note that this hyperbolic version is easier to compute than the dispersive formula (3.27). In the

latter the function ζ depends on the frequency ω. Therefore the Fourier-type integral in a_β cannot be computed rapidly by using the FFT (fast Fourier transform). On the other hand, the integral in (3.30) can be easily evaluated by the FFT algorithm because in this case the coefficient $r(x)$ is frequency-independent. In Appendix B we detail the numerical computation of the Fourier-type integral in coefficient $a_\beta(x_o, \omega)$. The accuracy of approximation (3.30) will be verified in section 4 showing that the leading-order dispersive effects are controlled by coefficient $b(x_o, \omega)$.

The numerical experiments in section 4 will show that approximation (3.29) captures very well not only the wave front but also part of the forward scattering radiation. The parameter X in (3.27) (or (3.30)) regulates to what extent the incoherent signal is recovered.

If $\beta = 0$, then $b(x_o, \omega) \equiv 0$, and the approximation given by (3.26) reduces to

$$\widehat{R}(x_o, \omega) \approx \widehat{f}(\omega) e^{-x_o a_0(x_o, \omega)}, \tag{3.31}$$

where

$$a_0(x_o, \omega) = \frac{1}{x_o} \int_0^{x_o} \int_x^{x+X} r(x) e^{2i\omega(x-x')} r(x') dx' \, dx,$$

as in Berlyand and Burridge's work [3]. We recall that when $\beta \neq 0$, the hyperbolic medium's correlation function $a_0(x_o, \omega)$ (which controls the attenuation mechanism) is altered and an extra attenuation term $b(x_o, \omega)$ appears due to the model's dispersion.

4. Numerical validation of the generalized ODA theory. Consider the nonlinear terrain-following Boussinesq system deduced by Nachbin [23],

$$\begin{aligned} &M(\xi)\eta_t + \left(\left(1 + \frac{\alpha\eta}{M(\xi)} \right) u \right)_\xi = 0, \\ &u_t + \eta_\xi + \frac{\alpha}{2} \left(\frac{u^2}{M(\xi)^2} \right)_\xi - \frac{\beta}{3} u_{\xi\xi t} = 0. \end{aligned} \tag{4.1}$$

We recall that when $\alpha = 0$, system (4.1) reduces to (2.5). Nevertheless, for our numerical validation experiments we will use the nonlinear Boussinesq system in a small α regime. Two types of initial data are considered. We study the propagation of Gaussian-shaped disturbances of the form

$$u(\xi, 0) = \eta(\xi, 0) = e^{-(\xi - \xi_o)^2/\epsilon},$$

where the parameter ξ_o controls the pulse's initial position and $\epsilon > 0$ its effective width. Furthermore, we also consider solitary waves of the form

$$\begin{aligned} \eta(\xi, 0) &= A_1 \, \mathrm{sech}^2(B(\xi - \xi_o)) + A_2 \, \mathrm{sech}^4(B(\xi - \xi_o)), \\ u(\xi, 0) &= A \, \mathrm{sech}^2(B(\xi - \xi_o)), \end{aligned}$$

with A_1, A_2, A, and B constants (to be defined in Experiment 2). These are approximate solutions to system (4.1) with $M \equiv 1$ (see [28]).

Except in some special cases (for instance, when $M \equiv 1, \alpha = 0$, or $\beta = 0$), finding the solution of system (4.1) is a nontrivial problem. To solve system (4.1) numerically we will use a finite difference solver introduced by Wei and Kirby [28]. This scheme will be used to perform numerical experiments in order to validate the theory developed in the previous sections.

First we rewrite system (4.1) in a more convenient way, as

$$\begin{aligned} \eta_t &= E(u,\eta), \\ V_t &= F(u,\eta), \end{aligned} \tag{4.2}$$

where

$$\begin{aligned} E(u,\eta) &= -\frac{1}{M(\xi)}\left(\left(1+\frac{\alpha\eta}{M(\xi)}\right)u\right)_\xi, \\ F(u,\eta) &= -\eta_\xi - \frac{\alpha}{2}\left(\frac{u^2}{M(\xi)^2}\right)_\xi, \end{aligned} \tag{4.3}$$

and V is an intermediate variable defined by

$$V = u - \frac{\beta}{3}u_{\xi\xi}.$$

To evaluate the boundary values we use the radiation conditions by Engquist and Majda (see [8])

$$\begin{aligned} u_t - u_\xi &= 0 \quad \text{at} \quad \xi = \xi_{\min}, \\ u_t + u_\xi &= 0 \quad \text{at} \quad \xi = \xi_{\max}, \end{aligned} \tag{4.4}$$

where $\xi_{\min}$ and $\xi_{\max}$ denote the left and right ends, respectively, of the computational domain.

The evolution system above is solved by using an efficient predictor-corrector scheme. The $V \to u$ change of variables is done with an efficient (tridiagonal) ODE numerical scheme. Details, numerical properties, and further numerical experiments are presented elsewhere [20, 21].

We now describe several experiments validating the dispersive pulse-shaping ODA theory.

Experiment 1 (Flat channel and effectively linear regime). In these experiments the pulse is assumed to propagate over a flat bottom ($M \equiv 1$). In Appendix A (cf. (A.6) and (A.7)) we show that if, in addition, $\alpha = 0$, we can explicitly solve system (4.1) by using the Fourier transform technique. Flat channel solutions are employed to verify the numerical method's accuracy regarding dispersive and stability properties.

In Figure 4.1 we see that the exact solution η (for $\alpha = 0$, $\beta = 0.03$) and the numerical solution (for $\alpha = 0.001$, $\beta = 0.03$) are in very good agreement at $t = 40$. After 40 length-units into the flat channel, the right-propagating Gaussian has developed an Airy-like oscillatory tail (cf. Appendix A). The dispersive properties of the numerical scheme are very good.

For this experiment the numerical parameters are $J = 4000$ (spatial mesh points; $\Delta\xi = 0.0125$) and $N = 5000$ (time mesh points; $\Delta t = 0.008$). As mentioned above, this test shows that the code is capturing the (effectively linear) dispersive regime very well when α is small enough.

We repeat the experiment above for $\alpha = 0.001$, $\beta = 0.0005$, and $t = 40$. Dispersion has been decreased substantially. Now the effective hyperbolic regime is clearly observed in Figure 4.2.

Radiation conditions (4.4) also proved to absorb appropriately waves leaving the computational domain. It was observed that reflected waves produced by the computational boundaries were negligible.

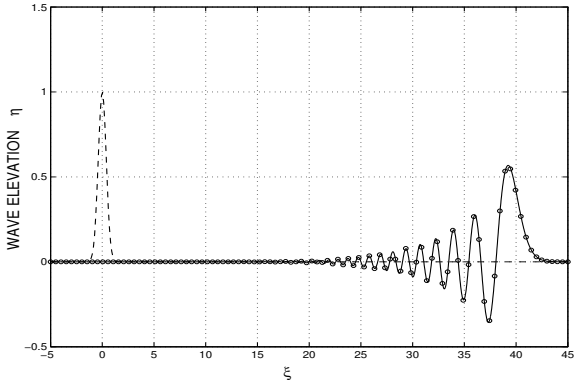

FIG. 4.1. *Dashed line: initial pulse,* $\eta(\xi,0) = u(\xi,0) = e^{-\xi^2/0.3}$. *Solid line: numerical solution for* $\alpha = 0.001$, $\beta = 0.03$, *and* $t = 40$. *Open circles: exact solution.*

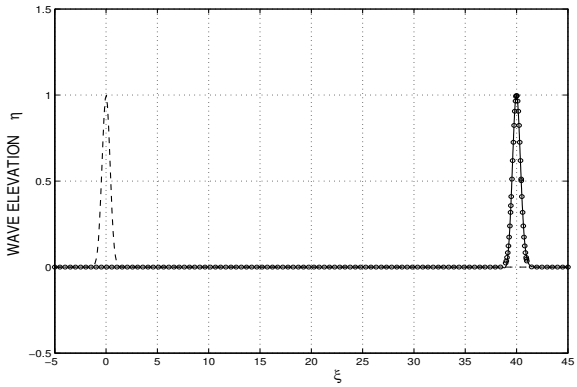

FIG. 4.2. *Dashed line: initial disturbance,* $\eta(\xi,0) = u(\xi,0) = e^{-\xi^2/0.3}$. *Solid line: numerical solution for* $\alpha = 0.001$, $\beta = 0.0005$, *and* $t = 40$. *Open circles: initial Gaussian pulse translated to* $\xi = 40$.

Experiment 2 (Flat channel and weakly nonlinear regime/solitary wave). We now study system (4.1) in the case that $M \equiv 1$, $0 < \alpha \ll 1$ (weakly nonlinear regime), and $0 < \beta \ll 1$ (weakly dispersive regime). Under these hypotheses it is possible to obtain an approximate solution of system (4.1) which has the analytical form

$$\begin{aligned} \eta(\xi,t) &= A_1 \operatorname{sech}^2(B(\xi - Ct - \xi_o)) + A_2 \operatorname{sech}^4(B(\xi - Ct - \xi_o)), \\ u(\xi,t) &= A \operatorname{sech}^2(B(\xi - Ct - \xi_o)), \end{aligned} \tag{4.5}$$

where

$$A_1 = \frac{C^2-1}{\alpha C^2} = \frac{1}{C^2}, \quad A_2 = \frac{(C^2-1)^2}{\alpha C^2} = \frac{\alpha}{C^2}, \quad C = \sqrt{1+\alpha}, \quad A = \frac{C^2-1}{\alpha C} = \frac{1}{C},$$

and

$$B = \left\{ \frac{C^2-1}{(4/3)\beta C^2} \right\}^{1/2} = \left\{ \frac{\alpha}{(4/3)\beta C^2} \right\}^{1/2}.$$

Note that $A_1 + A_2 = 1$. See Wei and Kirby [28] for details.

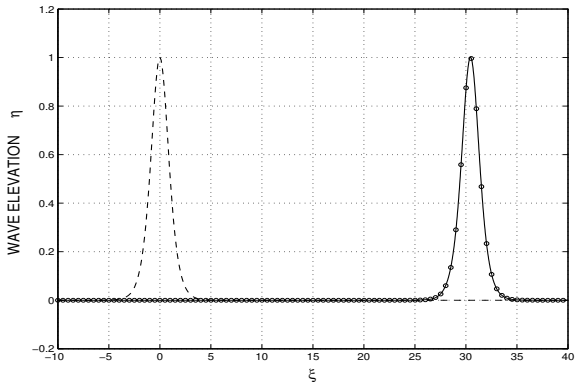

FIG. 4.3. *Solitary wave propagating over a flat bottom. Dashed line: initial disturbance* $\eta(\xi,0) = A_1\ sech^2(B\xi) + A_2\ sech^4(B\xi)$. *Solid line: numerical solution for* $\alpha = 0.03$, $\beta = 0.03$, *and* $t = 30$. *Open circles: analytical solution* (4.5).

In Figure 4.3 we show the analytical solution η given by (4.5) for $\alpha = \beta = 0.03$ and $t = 30$. The initial soliton position is set to be $\xi_o = 0$. The numerical solution is also included in this plot. The numerical parameters are $J = 2000$, $N = 2500$, $\Delta\xi = 0.025$, $\Delta t = 0.012$. Note that we have the same dispersion level as in the first simulation presented in Experiment 1. Now weak nonlinearity prevents the formation of an oscillatory tail.

Observe that the pulse's propagation velocity is $C \approx 1.0149$, in agreement with solution (4.5). The code reproduces very well the weakly dispersive, weakly nonlinear evolution of the soliton.

Experiment 3 (Disordered orography/hyperbolic regime). In Experiments 1 and 2, in which the channel's bottom was assumed to be flat, the orography-dependent coefficient $M(\xi)$ was taken to be $M \equiv 1$. For variable depths the computation of function $M(\xi)$ involves the solution of a change-of-variables problem (conformal mapping), which is not an easy task. For this reason, in next experiments, the smooth orography coefficient $M(\xi)$ will be synthesized directly as a piecewise linear function, ignoring (for the time being) its dependence on the original orography. In [20] we describe in detail how a numerical conformal mapping tool [6] is used in order to obtain a "nonsynthetic" $M(\xi)$. Nevertheless, synthetic $M(\xi)$ proves to be useful (i.e., efficient) for observing the phenomena we are interested in and for validating the theory. The synthesized orography coefficient is conceived as

$$M(\xi) = 1 + \delta\mu(\xi/\ell),$$

where μ is a mean-zero coefficient constructed using a random number generator. The fluctuation level is indicated by δ and its correlation length by ℓ. In the following experiments we use $\delta = 0.5$ and $\ell = 0.1$.

The numerical experiments are performed over a channel defined in the interval $[-15, 70]$. The fluctuations of the synthetic coefficient $M(\xi)$ cover the interval [5, 45]. The data for the right-propagating Gaussian is such that $\xi_o = -5$ and $\epsilon = 0.05$. The numerical solution is plotted as a function of the time-delay variable τ after propagating over 20 units of length and is presented in Figure 4.4. Note the wave

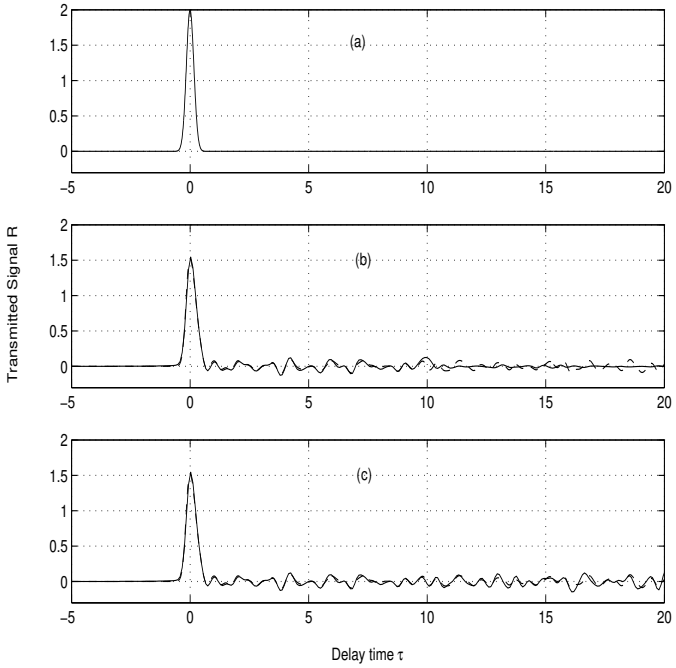

FIG. 4.4. *Pulse propagating over a synthetic disordered rapidly varying topography.* (a) *Initial disturbance* $R(0,\tau) = 2e^{-\tau^2/0.05}$. (b) *Solid line: ODA approximation* (3.31) *for* $X = 5$*; dashed line: numerical solution for* $\alpha = 0.001$, $\beta = 0$ *at* $\xi = 20$. (c) *Solid line: ODA approximation* (3.31) *for* $X = 20$*; dashed line: numerical solution at* $\xi = 20$ *and* α, β *as in* (b).

attenuation due to the orographic forcing. The transmitted signal has amplitude 1.5 (smaller than 2.0, the initial amplitude). The agreement between the numerical solution of the full nonlinear equations (with small α) and the linear theory is very good (Figure 4.4(b)). We also point out an outstanding feature of the theory, not noticed in previous work [3]. The linear hyperbolic ODA approximation is able to capture the forward scattering radiation, which is the incoherent coda behind the transmitted Gaussian. Theory and numerical experiment agree over the delay time interval up to approximately $\tau = 10$.

To verify the robustness of the theory we increase the size of the disordered medium's slab used in the invariant imbedding theory (namely, the variable X). In Figure 4.4(c) we plot the same numerical solution as above but compared with a theoretical result using an increased slab size (up to $X = 20$). The approximate theory captures an even larger segment of the forward scattering radiation beyond $\tau = 15$.

Experiment 4 (Disordered orography/dispersive regime). This set of experiments is important for two reasons. (A) It shows that we are able to properly compute the interaction of dispersive water waves with rapidly varying orographies. With previously known Boussinesq models (such as [26]) this was not possible. The classic Boussinesq equation [26] is not valid for orographies with large slopes. Moreover, its variable coefficient multiplies the highest derivative term, and this generates numerical noise as the orography's slope increases. This has been shown for a periodic topography in [20]. The same experiment was performed for the terrain-following

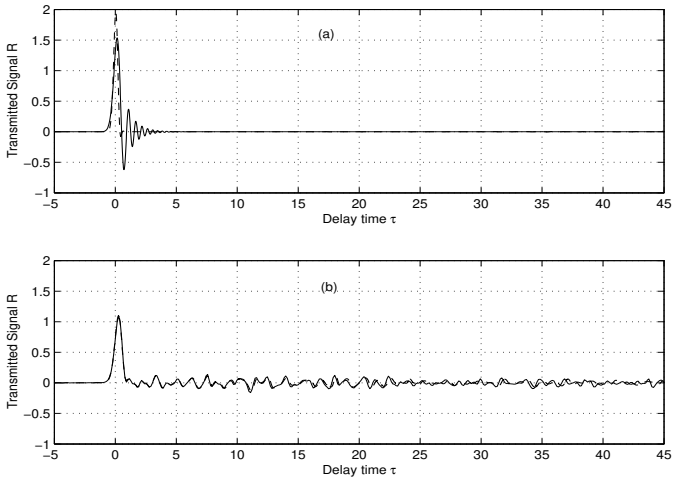

FIG. 4.5. (a) *Dashed line: initial disturbance. Solid line: solution for* $M \equiv 1$ *(flat bottom) at* $\xi = 40$. (b) *Pulse propagating over a synthetic disordered rapidly varying orography. Dashed line: numerical solution at* $\xi = 40$. *Solid line: generalized ODA approximation* (3.29) *for* $X = 20$. *In all experiments* $\alpha = 0.001$, $\beta = 0.0005$.

Boussinesq system where the metric term is positioned away from the third order (dispersive) term. No numerical noise was observed. (B) We illustrate the theoretical results in the regime for which they were deduced. Hence these linear experiments validate the nonlinear numerical model for the terrain-following Boussinesq equation in the presence of a random orography. This is important also since the code will be used (as a scientific computing tool) beyond the regime of validity of the linear theory.

In the first experiment we consider the dispersion to be very weak ($\beta = 0.0005$). Figure 4.5(a) clearly shows that a very short oscillatory tail develops when the pulse propagates in a flat channel. The final amplitude of the transmitted pulse is about 1.5. The amplitude decay in this case is entirely due to dispersion, as discussed in Appendix A, through the Airy kernel. However, in the presence of orographic forcing an additional attenuation is observed (Figure 4.5(b)). In this case the final amplitude is about 1. Note that no Airy-like oscillatory tail develops. This was systematically observed in several experiments and can be explained through the concept of *localization* [24]. The localization length of a Fourier mode is a *characteristic propagation distance* after which the transmission coefficient is negligible. The bulk of the energy is in the reflected signal. Moreover, high frequency components have small localization lengths. This means they are quickly filtered (back) by the disordered medium. In the context of the ODA theory this was phrased in a slightly different way by Berlyand and Burridge [3]. They called a layered random medium a *stratigraphic Gaussian filter*. As presented here, the transmitted pulse can be written as the convolution of its initial Fourier content with a Gaussian kernel. The Gaussian kernel is the leading-order approximation to the kernel in (3.29) with $\beta = 0$ (see [20, 21]). Applying this notion to our current problem, we have that disorder filters the higher part of the Fourier content of the incoming pulse. Hence the oscillatory tail (which is of high frequency content) has been converted into the incoherent part of the wave. Again the agreement between the numerical solution and the ODA theory is very good.

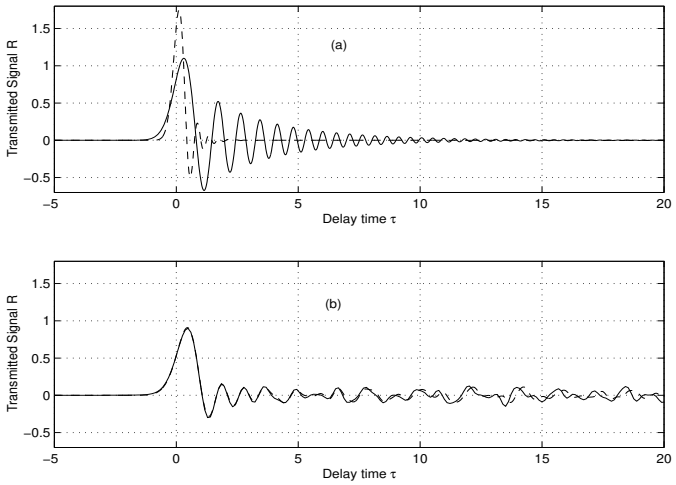

FIG. 4.6. (a) *Dashed line: initial disturbance. Solid line: solution for* $M \equiv 1$ *(flat bottom) at* $\xi = 40$. (b) *Pulse propagating over a synthetic disordered rapidly varying orography. Dashed line: numerical solution at* $\xi = 40$. *Solid line: generalized ODA approximation* (3.29) *for* $X = 20$. *In all experiments* $\alpha = 0.001$, $\beta = 0.002$.

In the next validation experiment the level of dispersion has been increased four times ($\beta = 0.002$). In Figure 4.6(a) we have the initial pulse profile and the numerical solution after propagation over 40 units of a flat channel. We observe a long oscillatory tail due to the higher dispersion level. Note that dispersion is not as small as the value of β might indicate at first sight. After large propagation distances the (small) phase lag (at higher frequencies) has accumulated in a nontrivial fashion.

To compute the theoretical ODA approximation we need the incoming pulse in time at the origin. Actually we need its Fourier content $\hat{f}(\omega)$. To be consistent with our mathematical theory we position the initial Gaussian profile (in space) to the left of the origin at time t_o, allow it to propagate over a flat portion of the channel, and record it in time at the origin. The starting time t_o is chosen so that the resulting pulse $f(\tau)$ will be centered at $\tau = 0$. This gives us the correct incoming pulse (in time) for the theoretical formula to be used. Hence the incoming pulse displays a mild oscillatory tail as displayed by Figure 4.6(a). In Figure 4.6(b) we compare the numerical solution with the generalized ODA approximation. The dispersive wave attenuation can again be observed, in particular if we examine the envelope of the Airy-like solution.

Experiment 5 (Disordered orography/solitary wave). We are now in a position to explore the (linear) generalized ODA theory beyond its regime of validity. We consider a weakly nonlinear weakly dispersive wave, namely a soliton. Using (4.5), it is easy to see that we have

$$f(\tau) = \left(\frac{1}{C^2} + \frac{1}{C}\right) \operatorname{sech}^2(B\tau) + \frac{\alpha}{C^2} \operatorname{sech}^4(B\tau)$$

in order to evaluate the ODA approximation (3.29).

In order to slowly push away from the regime of validity of our theory we choose small values for the respective parameters $\alpha = \beta = 0.001$. This amount of dispersion

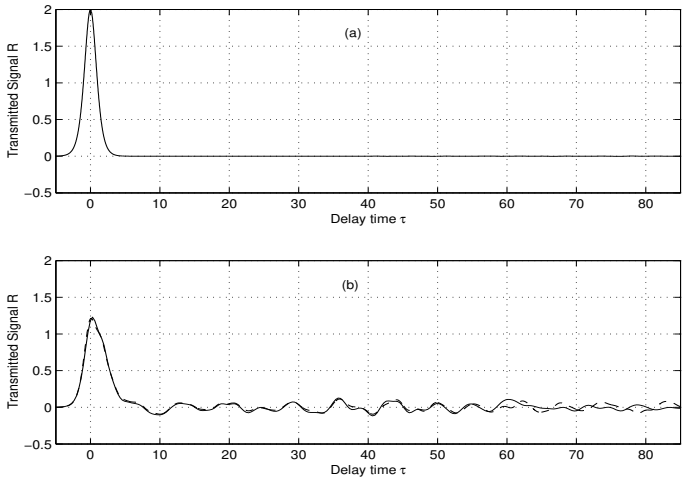

FIG. 4.7. *Soliton propagating over a synthetic disordered rapidly varying orography.* (a) *Initial soliton* $f(\tau)$. (b) *Dashed line: numerical solution for* $\alpha = 0.001$, $\beta = 0.001$ *at* $\xi = 150$. *Solid line: generalized ODA approximation* (3.29) *for* $X = 30$.

is enough to produce an oscillatory coda, as was observed in previous experiments. But now, for the particular data considered, this coda will not appear due to the perfect balance between the α and β terms. The oscillatory coda seen in Figure 4.7(b) is due entirely to forward scattering of energy generated by the interaction of the soliton with the disordered medium. Because the soliton is wider than the Gaussian (used before) we adopt $\ell = 0.6$. This keeps the wave/inhomogeneities ratio equal to approximately 10 ($\gamma = 0.1$) as in all other experiments. The orography coefficient covers the [5, 245] interval, and the amplitude of fluctuations is $\delta = 0.5$. In Figure 4.7(b) we present the excellent agreement between the theory and the numerical solution.

It is worthwhile recalling that the solitary wave (4.5) is an approximate solution to the Boussinesq equations as presented by Wei and Kirby [28] in their appendix. In [28, p. 255] they discuss solitary-wave propagation over a flat bottom and analyze the effects, under the corresponding approximation, of increasing the soliton's amplitude (namely, the nonlinearity parameter α, denoted there by δ). They observed that for $\alpha = 0.1$ the initial profile specified by (4.5) undergoes a rapid adjustment to a slightly higher solitary wave with a very small dispersive tail. This dispersive tail is not noticeable in their experiment [28, Figure 2(a)] after the soliton has propagated over 55 pulsewidths (450 length units). Nevertheless the amplitudes of the tail and of the rapid deviation from the initial solitary wave height both increase with increasing α. As explained in [28], this is partially because the fourth-order ODE used to develop the analytical solution is only asymptotically equivalent to the Boussinesq model used in the computations. In particular, for $\alpha = 0.3$ Wei and Kirby show that the corresponding evolution for (4.5) is far from a traveling wave solution.

As pointed out before, the ODA theory developed is linear, while these experiments are performed beyond the linear regime. Hence in our experiments we will gradually increase the values of α, but we will be far from the "problematic regime" indicated by Wei and Kirby [28]. In our second experiment with solitons, and to

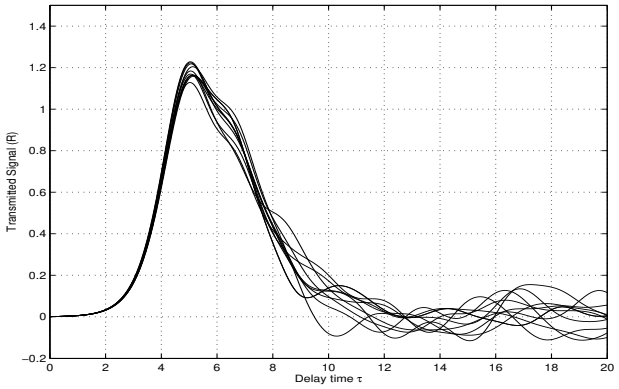

FIG. 4.8. *Transmitted pulse stabilization observed at a fixed medium's station ($\xi = 150$; 25 pulse widths). The same initial soliton ($\alpha = \beta = 0.002$) propagated over ten different realizations of the topography. The transmitted pulse shape is effectively deterministic, while the coda is random.*

further move away from the linear regime, we double the nonlinearity and dispersive parameters accordingly. We will now investigate the effect of different realizations of the medium. In Figure 4.8 we present the results for ten different realizations of the disordered topography. We observe the stabilization of the transmitted pulse: the pulse shaping of the front is independent of the specific realization. This has been proved for the linear hyperbolic case [15]. Stabilization in the linear dispersive regime has been recently proved in [10]. The present framework has been extended, through a stochastic analysis, to include stabilization [10] for the time-reversed refocusing of dispersive waves. No stabilization theory is yet available for solitons though.

As already mentioned, the solitary wave profile (4.5) is not an exact traveling wave solution to the corresponding, constant coefficient, Boussinesq system. Nevertheless the balance between weak nonlinearity and weak dispersion is maintained for large time intervals. If dispersion were not present, a Burgers-type nonlinearity ($\eta_t + \alpha\eta\eta_x = 0$) would force the solitary wave profile (4.5) to eventually break. For an initial profile denoted as $\eta(x,0) = f(x)$ the critical time t_c is known to be $t_c = -1/(\alpha f')$ for the maximum value of the negative slope of $f(x)$. For $f(x)$ given by (4.5), with $\alpha = \beta = \varepsilon$, the maximum value of the negative slope is at $\tilde{x}$ such that $\tanh(B\tilde{x}) = -z$, where

$$z = \left(\frac{1 + C + 2\alpha}{3 + 3C + 10\alpha}\right)^{1/2},$$

$$f'(\tilde{x}) = -\left(\frac{3}{(1+\varepsilon)^3}\right)^{1/2}\left[\frac{1-z^2}{z^2}\left((1+C)z + 2\varepsilon\left(\frac{1-z^2}{z}\right)\right)\right], \quad \text{with} \quad C = \sqrt{1+\varepsilon},$$

and $t_c \approx 1/(4\varepsilon)$. Hence if dispersion were switched off, the solitary wave would break after 50 length units (approximately 8.33 pulse widths), when $\varepsilon = \alpha = 0.005$, as will be used in the following experiment.

In our last experiment we further increase nonlinearity and dispersion to $\alpha = \beta = 0.005$. The result is presented in Figure 4.9. As observed in Experiment 4, disorder attenuates the effect of dispersion in this weakly nonlinear experiment. Note the soliton steepening at the wave front due to the attenuation of the dispersive mechanism. The attenuated wave front predicted by the linear theory does not match

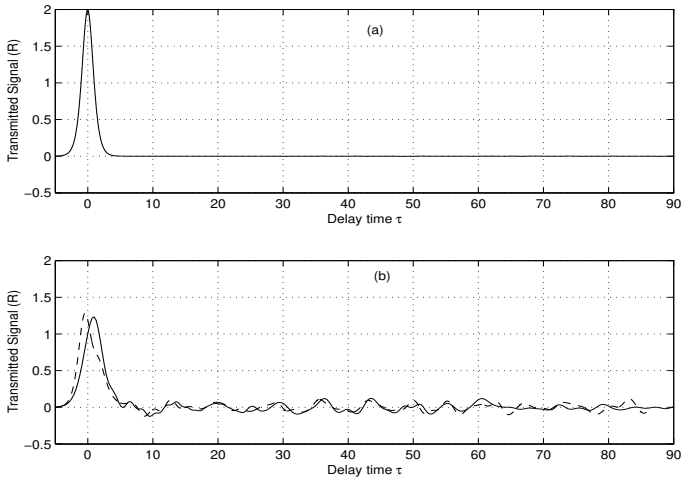

FIG. 4.9. *Soliton propagating over a synthetic disordered rapidly varying orography.* (a) *Initial soliton* $f(\tau)$. (b) *Dashed line: numerical solution for* $\alpha = 0.005$, $\beta = 0.005$ *at* $\xi = 150$. *Solid line: generalized ODA approximation* (3.29) *for* $X = 30$.

the nonlinear numerical front as before. Note also that dispersion has not been fully switched off or else a shock would have formed in finite time according to the discussion above. More experiments with solitary waves, including time-reversal and refocusing, are presented in [20].

The study of solitary waves moving over disordered topography is of great interest. In this work we have presented only scientific computing results. A complete theoretical understanding is of interest and will be considered in the future. Recently progress has been made in this direction [10, 11]. Theoretical results for nonlinear localization and soliton propagation in random media are recent and more focused on the nonlinear Schrödinger (NLS) equation. A very good source of references can be found through the work of Garnier [12, 13]. We are not aware of any results regarding solitons for the Boussinesq system (or equation).

5. Conclusion. We have formulated a generalization of the ODA theory for linear weakly dispersive waves. The theory has been validated numerically and pushed beyond its linear regime of validity. In particular, both the theoretical expressions and the numerical experiments have been able to capture the apparent diffusion of small amplitude solitary waves. This is a theme of great interest: soliton propagation in disordered media. Further mathematical analysis is needed to fully understand this problem.

Nevertheless this work has stimulated new theoretical results in the stochastic formulation for time-reversed dispersive wave refocusing [10] and also for the ODA and time-reversed refocusing [11] of weakly nonlinear hyperbolic waves. The authors [11] have shown that, to leading order, the transmitted pulse is governed by a viscous Burgers equation. The "apparent viscosity" depends on statistics of the random medium. This important result reports on a weakly nonlinear ODA theory for nondispersive waves. Therefore the regularizing effect is entirely due to the "apparent viscosity" promoted by the disordered orography. But it still does not apply to solitons. Details of the "apparently viscous" theory, including additional nonlinear experiments, are presented in [11].

Appendix A. Solutions for the linear KdV equation and the linear Boussinesq model.

The linear KdV equation. Consider the initial value problem

$$u_t + u_x + \gamma u_{xxx} = 0, \tag{A.1}$$

$$u(x,0) = f(x), \tag{A.2}$$

where γ is a nonzero constant. Using a Fourier transform in x, the solution for (A.1) and (A.2) is given by

$$u(x,t) = \frac{1}{2\pi}\int_{-\infty}^{\infty}\left(\int_{-\infty}^{\infty} e^{i(k(x-t-y)+\gamma k^3 t)}dk\right) f(y)dy. \tag{A.3}$$

Making a convenient change of variables, the inner integral in (A.3) can be expressed in terms of the Airy function to give

$$u(x,t) = \frac{1}{(3t\gamma)^{1/3}}\int_{-\infty}^{\infty} \mathrm{Ai}\left(\frac{x-t-y}{(3t\gamma)^{1/3}}\right) f(y)dy. \tag{A.4}$$

The Airy kernel gives the rate in time at which a pulse $f(x)$ will spread due to dispersion. This is useful information for the invariant imbedding technique used in the ODA theory.

The linear Boussinesq model. Now we study the linearization of system (4.1) for constant depth:

$$\begin{aligned} &\eta_t + u_\xi = 0,\\ &u_t + \eta_\xi - \frac{\beta}{3}u_{\xi\xi t} = 0, \end{aligned} \tag{A.5}$$

with the initial conditions

$$\eta(\xi,0) = u(\xi,0) = f(\xi).$$

Analogously to the KdV equation, we can apply the Fourier transform technique to obtain the Fourier coefficients

$$\begin{aligned} \hat{\eta}(k,t) = \frac{\hat{f}(k)}{2}\Bigg[&\left(1-\sqrt{1+(\beta/3)k^2}\right)e^{\frac{ikt}{\sqrt{1+\beta/3k^2}}}\\ &+\left(1+\sqrt{1+(\beta/3)k^2}\right)e^{\frac{-ikt}{\sqrt{1+\beta/3k^2}}}\Bigg], \end{aligned} \tag{A.6}$$

$$\begin{aligned} \hat{u}(k,t) = \frac{\hat{f}(k)}{2\sqrt{1+(\beta/3)k^2}}\Bigg[&\left(1+\sqrt{1+(\beta/3)k^2}\right)e^{\frac{-ikt}{\sqrt{1+\beta/3k^2}}}\\ &-\left(1-\sqrt{1+(\beta/3)k^2}\right)e^{\frac{ikt}{\sqrt{1+\beta/3k^2}}}\Bigg]. \end{aligned} \tag{A.7}$$

We point out that in the hyperbolic case ($\beta = 0$) the above initial data gives rise to (only) a right-propagating mode. In the dispersive case a negligible left-propagating mode is always present in this type of data. Notice that, because of (A.6), (A.7), and

$$\frac{1}{\sqrt{1+(\beta/3)k^2}} = 1 - (k^2/6)\beta + O(\beta^2),$$

we have that

$$\widehat{L}(t,k) = \hat{\eta}(t,k) - \hat{u}(t,k) = O(\beta) \approx 0,$$

provided that β is small enough. For the hyperbolic case the left-propagating mode is identically zero.

The dispersion relation for system (A.5) is

$$\omega_{\pm} = \omega_{\pm}(k) = \pm \frac{k}{\sqrt{1 + \frac{\beta}{3}k^2}}, \tag{A.8}$$

where ω_+ and ω_- represent Fourier modes propagating to the right and left, respectively. In contrast to the KdV equation, the phase velocity is

$$C_k^{\pm} = \frac{\omega_{\pm}}{k} = \pm \frac{1}{\sqrt{1 + \frac{\beta}{3}k^2}},$$

which does not switch signs and is bounded by one. Furthermore, $\omega_+ = \omega_+(k)$ coincides up to $O(k^3)$ with the dispersion relation for the KdV equation above with $\gamma = \beta/6$. Note also that, for waves generated in space, the range of possible time frequencies is bounded by $(3/\beta)^{1/2}$ for all k. As a consequence, solutions u, η of system (A.5) are band-limited functions in t. This fact justifies why frequencies ω higher than $\sqrt{3/\beta}$ are not considered in the analysis presented in section 3.

Appendix B. Numerical computation of coefficients $a_\beta(x_o, \omega)$ and $b(x_o, \omega)$. As mentioned in section 3, the numerical computation of the dispersive coefficient $a_\beta(x_o, \omega)$ is expensive. To override this difficulty, and use the FFT, we approximated $a_\beta(x_o, \omega)$ by the hyperbolic medium's correlation function $a_0(x_o, \omega)$, which corresponds to the leading-order term of a Taylor series expansion of a_β around $\beta = 0$. The numerical experiments in section 4 showed the high accuracy of this approximation.

To compute coefficient $a_0(x_o, \omega)$ as in (3.30) we rewrite it as

$$a_0(x_o, \omega) = \int_0^X \Phi(\eta) e^{-2i\omega\eta} d\eta, \tag{B.1}$$

where

$$\Phi(\eta) = \frac{1}{x_o} \int_0^{x_o} r(x) r(x + \eta) dx.$$

We know by the correlation theorem that

$$\int_{-\infty}^{\infty} r(x) r(x + \eta) dx = F^{-1}[\hat{r}\bar{\hat{r}}](\eta),$$

where the hat denotes the Fourier transform, F^{-1} the inverse Fourier transform, and the bar indicates complex conjugation. Therefore function Φ defined above can be computed by using the FFT algorithm, letting the coefficient $r(x)$ be zero outside the interval $[0, x_o]$. This is consistent with the invariant imbedding approach. We must append enough zeros to the tail of the sampled coefficient $r(x)$ (zero padding) in order

to eliminate the overlapping phenomenon that appears due to the fact that $r(x)$ is not a periodic function. The FFT assumes periodicity in both physical and frequency domains (see Brigham [4]). The cost of computing the discrete correlation function results in only three FFT evaluations, which is faster than an ordinary computation of the integral defining Φ for each value of η. The numerical code to perform the discrete correlation can be found in [4].

Once the function Φ is known, the windowed Fourier transform in (B.1) is evaluated by using only one FFT. Analogously to the discrete correlation, zero padding outside the interval $[0, X]$ is required on the sampling of function Φ.

To evaluate the generalized ODA approximation presented in section 3 we also need the dispersive coefficient $b(x_o, \omega)$. To make its computation faster we rewrite it in the more compact form

$$b(x_o,\omega) = -\frac{\beta}{6x_o}\int_0^{\xi(x_o)} \frac{-i\omega^3 M^{3/2}(\xi) + M'(\xi)\omega^2}{1-(\beta/3)M(\xi)\omega^2}\,d\xi, \tag{B.2}$$

where the upper limit $\xi(x_o)$ denotes the spatial position in the medium corresponding to the travel time x_o. Thus we need compute only once the coefficients $M(\xi)$, $M^{3/2}(\xi)$, and $M'(\xi)$, which can be stored at the beginning. The integral in (B.2) is approximated by the trapezoidal method for roughly 2^{14} frequencies in the range $|\omega| < C_o(x_o)\sqrt{3/\beta}$. Since $b(x_o, -\omega) = \overline{b(x_o, \omega)}$, only positive frequencies need to be evaluated.

Appendix C. Error estimation of the pulse shaping theory. In section 3 the reflection kernel K was decomposed according to the result of Lemma 3.1. In the derivation of the generalized ODA approximation (under the hypotheses of rapidly varying orography and weakly dispersive regime $0 < \beta \ll 1$) we retained only the first term on the right-hand side of the decomposition, leading to the approximation

$$\widehat{K}(x,\omega) \approx -\int_x^{x+X} e^{2i\omega\int_{x'}^{x}\Gamma(s,\omega)\,ds}\bar{\zeta}(x',\omega)dx'. \tag{C.1}$$

We wish to give numerical evidence showing the accuracy of this approximation. First, observe that the reflection kernel K can be computed by solving numerically the Riccati equation

$$\widehat{K}_x = \bar{\zeta}(x,\omega) + 2i\omega\Gamma(x,\omega)\widehat{K} - \zeta(x,\omega)\widehat{K}^2,$$

subject to

$$\widehat{K}(x_o + X, \omega; T) = 0.$$

(See the definitions of coefficients Γ and ζ in section 3.) Consequently, we can evaluate the error function $E(x_o, \omega)$ at any time x_o and frequency ω. The results are presented in Figure C.1, where we compare the norm of function $E(x_o, \omega)$ to that of approximation (C.1) at point $\xi = 40$, with $X = 20$ and $\beta = 0.005$. We see that the error function is negligible over all frequencies. The parameters used for the orography considered here are $L = 240$ (total length of the rough bottom), $\ell = 0.6$ (scale of variation of the orography), and $\delta = 0.5$ (amplitude of orography's fluctuations).

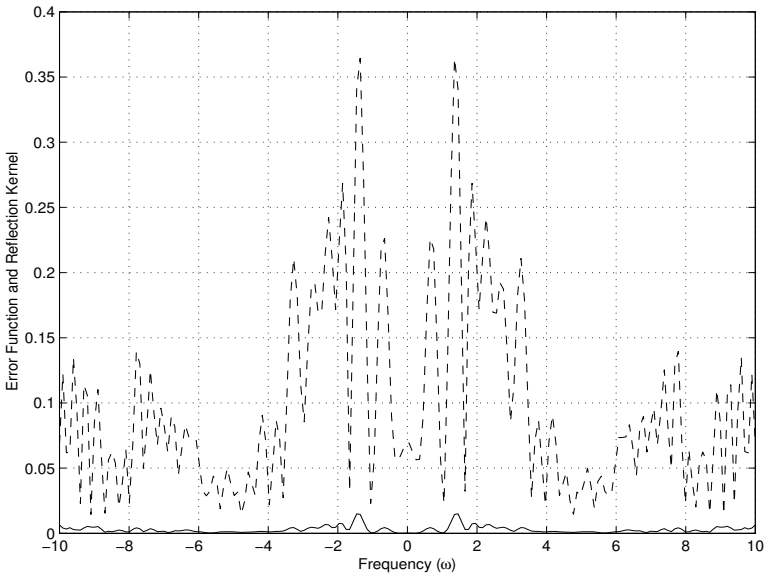

FIG. C.1. *Solid line: error norm for* $\beta = 0.005$, $X = 20$ *at* $\xi = 40$. *Dashed line: norm of approximation* (C.1) *for the same parameters.*

Acknowledgments. A. Nachbin is grateful to Prof. George Papanicolaou, as the chairman of the Mathematical Geophysics Summer School at Stanford, and for many useful discussions on this subject. He also thanks Prof. Robert Burridge for several helpful conversations regarding reference [3] during MGSS 1998.

REFERENCES

[1] M. ASCH, W. KOHLER, G. C. PAPANICOLAOU, M. POSTEL, AND B. WHITE, *Frequency content of randomly scattered signals*, SIAM Rev., 33 (1991), pp. 519–625.

[2] P. G. BAINES, *Topographic Effects in Stratified Flows*, Cambridge University Press, Cambridge, UK, 1995.

[3] L. BERLYAND AND R. BURRIDGE, *The accuracy of the O'Doherty–Anstey approximation for wave propagating in highly disordered stratified media*, Wave Motion, 21 (1995), pp. 357–373.

[4] E. O. BRIGHAM, *The Fast Fourier Transform and Its Applications*, Prentice-Hall, Englewood Cliffs, NJ, 1988.

[5] R. G. DEAN AND R. A. DALRYMPLE, *Water Wave Mechanics for Engineers and Scientists*, 3rd ed., World Scientific, River Edge, NJ, 1993.

[6] T. DRISCOLL, http://www.math.udel.edu/~driscoll/software.

[7] EUROPEAN CENTRE FOR MEDIUM-RANGE WEATHER FORECASTS (ECMWF), *Orography*, Proceedings of a Workshop held at ECMWF, Shinfield Park, Reading, UK, 1998.

[8] B. ENGQUIST AND A. MAJDA, *Absorbing boundary conditions for the numerical simulation of waves*, Math. Comp., 31 (1977), pp. 629–651.

[9] J. F. CLOUET AND J. P. FOUQUE, *Spreading of a pulse travelling in random media*, Ann. Appl. Probab., 4 (1994), pp. 1083–1097.

[10] J. P. FOUQUE, J. GARNIER, AND A. NACHBIN, *Time reversal for dispersive waves in random media*, SIAM J. Appl. Math., to appear.

[11] J. P. FOUQUE, J. GARNIER, AND A. NACHBIN, *Shock structure due to stochastic forcing and time reversal for nonlinear water waves in random media*, Phys. D, to appear.

[12] J. GARNIER, *Long-time dynamics of Korteweg–de Vries solitons driven by random perturbations*, J. Statist. Phys., 105 (2001), pp. 789–833.

[13] J. Garnier, *Exponential localization versus soliton propagation*, in Nonlinearity and Disorder: Theory and Applications (Proceedings of the NATO Advanced Research Workshop, Tashkent, Uzbekistan, 2001), F. Abdullaev, O. Bang, and M. P. Sørensen, eds., Kluwer Academic Publishers, Dordrecht, The Netherlands, Vol. 45, 2002, pp. 3–17.
[14] J. Hamilton, *Differential equations for long-period gravity waves on a fluid of rapidly varying depth*, J. Fluid Mech., 83 (1977), pp. 289–310.
[15] P. Lewicki, R. Burridge, and M. V. de Hoop, *Beyond effective medium theory: Pulse stabilization for multimode wave propagation in high-contrast layered media,* SIAM J. Appl. Math., 56 (1996), pp. 256–276.
[16] F. Mattioli, *Decomposition of the Boussinesq equations for shallow-water into a set of coupled Korteweg–de Vries equations*, Phys. Fluids A, 3 (1991), pp. 2355–2359.
[17] F. Mattioli, *On the Hamiltonian decomposition of the Boussinesq equations in a pair of coupled Korteweg–de Vries equations*, Wave Motion, 28 (1998), pp. 283–296.
[18] C. C. Mei, *The Applied Dynamics of Ocean Surface Waves*, John Wiley, New York, 1983.
[19] G. Meyer, *Initial Value Methods for Boundary Value Problems: Theory and Application of Invariant Imbedding*, Academic Press, New York, 1973.
[20] J. C. Muñoz Grajales and A. Nachbin, *Stiff microscale forcing and solitary wave refocusing*, Multiscale Model. Simul., submitted.
[21] J. C. Muñoz Grajales, *Dispersive Wave Attenuation and Refocusing Due to Disordered Orographic Forcing*, Ph.D. thesis (in English), Instituto de Matematica Pura e Aplicada, Rio de Janeiro, Brazil, 2002.
[22] A. Nachbin, *Modelling of Water Waves in Shallow Channels*, Computational Mechanics Publications, Southampton, UK, 1993.
[23] A. Nachbin, *A terrain-following Boussinesq system*, SIAM Appl. Math., 63 (2003), pp. 905–922.
[24] A. Nachbin, *The localization length of randomly scattered water waves,* J. Fluid Mech., 296 (1995), pp. 353–372.
[25] R. F. O'Doherty and N. A. Anstey, *Reflections on amplitudes*, Geophys. Prospecting, 19 (1971), pp. 430–458.
[26] D. H. Peregrine, *Long waves on a beach*, J. Fluid Mech., 27 (1967), pp. 815–827.
[27] G. Papanicolaou and K. Sølna, *Ray theory for a locally layered random medium*, Waves in Random Media, 10 (2000), pp. 151–198.
[28] G. Wei and J. Kirby, *Time-dependent numerical code for extended Boussinesq equations*, J. Waterway, Port, Coastal, and Ocean Engineering, 121 (1995), pp. 251–261.
[29] G. B. Whitham *Linear and Nonlinear Waves*, John Wiley, New York, 1974.